Available online at www.sciencedirect.com
SCIENCE DIRECT
Biochimica et Biophysica Acta 1746 (2005) 221 – 233
BIOCHIMICA ET BIOPHYSICA ACTA
BBA
http://www.elsevier.com/locate/bba

Review

Use of Forster's resonance energy transfer microscopy to study lipid rafts

Madan Rao [a,b,*], Satyajit Mayor [a,*]

[a] National Centre for Biological Sciences (TIFR), UAS-GKVK Campus, GKVK PO, Bellary Road, Bangalore 560 065, India
[b] Raman Research Institute, CV Raman Avenue, Bangalore 560 080, India

Received 20 April 2005; received in revised form 12 July 2005; accepted 11 August 2005
Available online 25 August 2005

Abstract

Rafts in cell membranes have been a subject of much debate and many models have been proposed for their existence and functional significance. Recent studies using Forster's resonance energy transfer (FRET) microscopy have provided one of the first glimpses into the organization of putative raft components in living cell membranes. Here we discuss how and why FRET microscopy provides an appropriate non-invasive methodology to examine organization of raft components in cell membranes; a combination of homo and hetero-FRET microscopy in conjunction with detailed theoretical analyses are necessary for characterizing structures at nanometre scales. Implications of the physical characteristics of the organization of GPI-anchored proteins in cell membranes suggest new models of lipid-based assemblies in cell membranes based on active principles.

Keywords: Raft; GPI-anchored protein; Homo-FRET; Hetero-FRET; Microscopy; Active organization

1. Introduction

1.1. Functional organization at different spatio-temporal scales

There is growing evidence that the multiple lipid and protein components of the plasma membrane of a living cell is organized, both compositionally and functionally, at different spatial and temporal scales. For instance, the construction of the Rab protein domains in membranes [1], the clathrin coated-pit [2,3], or the immunological synapse [4] are exquisite examples of functional compartmentalization in cell membranes for sorting and signaling purposes. A large variety of cellular functions carried out at the cell surface require a regulated spatio-temporal organization of cell surface components. Lipid rafts could represent similar membrane compartmentalization, or could facilitate some specific types of functional assemblies in membranes.

1.2. The 'raft' hypothesis

Lipid microdomains in living cells were proposed primarily to reconcile an intriguing observation that distinct lipid compositions at the apical and basolateral surfaces of morphologically polarized epithelial cells appear to be generated by sorting of lipids and proteins during traffic between the Golgi and cell surface [5]. The lipid raft microdomain model was envisaged to generate a mechanism for segregating and sorting newly-synthesized lipids at the Golgi for traffic to the distinct cell surfaces of a polarized epithelium.

In a provocative article, Simons and Ikonen proposed that lipid rafts are specialized regions of cell membrane where sphingolipids and cholesterol come together as a result of chemical affinity and/or their preferential packing [6]. These regions could include or exclude other lipids and proteins and this specific segregation was proposed to mediate their biological function. Lipid rafts have since been implicated in a variety of functions such as sorting, endocytosis, signaling and cell migration [7]. There is significant confusion in their definition, consequently, there is considerable debate about their existence, and their precise role in biological function [8]. Currently, a number of models have been proposed for rafts [9,10]. A common picture of membrane rafts envisages liquid

* Corresponding authors. M. Rao is to be contacted at Raman Research Institute, CV Raman Avenue, Bangalore 560 080, India. Tel.: +91 80 2361 1326; fax: +91 80 2363 6662. S. Mayor, tel.: +91 80 2363 6421; fax: +91 80 2363 6662.
E-mail addresses: mayor@ncbs.res.in (S. Mayor), madan@rri.res.in (M. Rao).

0167-4889/$ - see front matter © 2005 Elsevier B.V. All rights reserved.
doi:10.1016/j.bbamcr.2005.08.002

ordered domains in cell membranes enriched in cholesterol and sphingolipid (SL), with which certain proteins are likely to associate [6]. These structures are believed to be akin to the large scale (≥50 nm) phase segregated liquid ordered domains observed in ternary artificial membrane systems (~50 nm; see also [11]). Other researchers envisage rafts as 'lipid shells' [12]; small, dynamic molecular-scale assemblies in which 'raft' proteins preferentially associate with certain types of lipids which transform into functional structures by dynamic and regulated processes. Yet another point of view pictures rafts as a 'mosaic of domain' encompassing a large fraction of the cell membrane, which may be regulated via a cholesterol-based mechanism [13]. A different picture proposed by Mayor and Rao [9] envisages small and dynamic multimeric lipid assemblies coexisting with monomers, which are maintained actively by the cell surface. These preexisting structures maybe actively induced to form large-scale stable 'rafts'. These different viewpoints are summarized in Fig. 1.

1.3. Studying lipid rafts

Lipid rafts have been studied and defined by a variety of techniques, resulting in a number of different criteria to ascertain their existence [9,14]. A commonly used biochemical criterion has been association with membranes relatively resistant to cold non-ionic detergent extraction [15], termed detergent resistant membranes or DRMs. However if lipid rafts are indeed formed by lipid interactions, addition of detergents to the membrane is likely to cause major perturbations. It has been observed that inclusion of non-ionic detergents in artificial membranes promotes the formation of ordered membranes; it alters phase behavior in artificial membrane bilayers of similar lipid composition as DRM lipids [16–18]. Correlation of cellular processes with lipid composition of cell membranes (especially cholesterol or sphingolipid levels) has been another way of ascertaining the role of rafts in a given functional context [14,19]. Lipid depletion, especially acute cholesterol depletion, may have rather drastic consequences for cell physiology in general making it difficult to interpret perturbations of lipid rafts in isolation [20]. Therefore, neither DRM-association nor lipid depletion protocols provide unambiguous evidence for pre-existing lipid-dependent assemblies in living cell membranes.

Analyses of the protein composition of DRMs have provided a list of potential raft-associated molecules [21], with methodological caveats regarding their raft-association [22]. In an environment as complex as a cell membrane, DRM-association may at best serve to define a circumstantial biochemical characteristic. It cannot provide information regarding the pre-existing organization of membrane components on the multi-

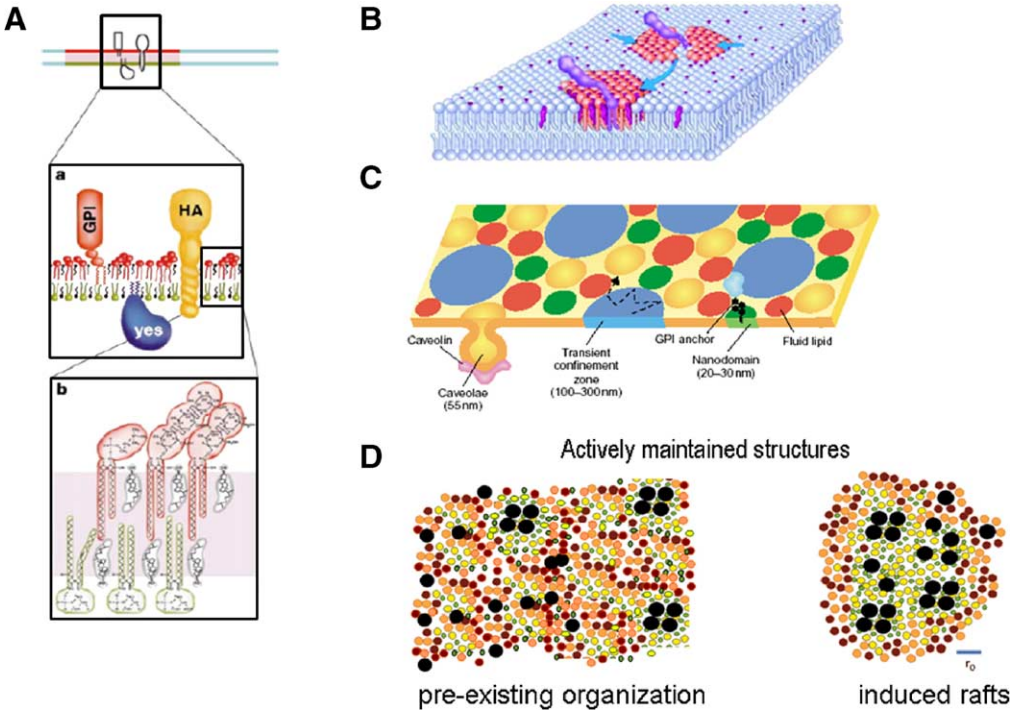

Fig. 1. (A) The most commonly cited hypothesis for membrane rafts proposed by K. Simons (Dresden, Germany) [6] depicts rafts that are relatively large structures (~50 nm; see also [11]), enriched in cholesterol and sphingolipid (SL), with which proteins are likely to associate. (B) Anderson and Jacobson [12] visualize rafts as lipid shells which are small, dynamic molecular-scale assemblies in which 'raft' proteins preferentially associate with certain types of lipids. The recruitment of these 'shells' into functional structures could be a dynamic and regulated process. (C) Another point of view is that a large fraction of the cell membrane is raft-like and exist as a 'mosaic of domains'; cells regulates the amount of the different types of domains via a cholesterol-based mechanism [13]. (D) Actively generated spatial and temporal organization of raft components. A different picture proposed in Mayor and Rao [9] suggests that in the steady state there are no functional 'rafts', instead small and dynamic lipid assemblies which co-exist with monomers are observed. These structures are then actively induced to form large-scale stable 'functional rafts'. Black circles, GPI-anchored proteins; red and pink circles, non-raft associated lipids; yellow circles, raft-associated lipids; green, cholesterol. Scale bar ~5 nm. [Figure reprinted from Ref. [9] with permission].

component cell surface, nor a quantitation of its physical characteristics.

Consider the case of lipid anchored proteins, specifically the family of glycosylphosphatidylinositol (GPI)-anchored proteins which lack any cytoplasmic extension, and where the sole membrane anchor is the glycolipid moiety. A major fraction of GPI-anchored proteins is DRM associated, however it would be difficult to account for the diverse characteristics exhibited by GPI-anchored proteins (sorting during endocytosis or trafficking in polarized cells [19,23]) by merely suggesting that they are associated with DRM's [24], and hence by implication, 'rafts'.

Experiments conducted in artificial membrane systems with compositions similar to that found in DRMs, show macroscopically segregated domains with characteristics of liquid ordered domains. This supports the idea that ordered lipid domains are more detergent resistant [25–27]. In contrast, in cell membranes although DRMs are routinely isolated, there is little evidence for such large scale segregation unless the membrane is severely perturbed [28].

All of the above imply that non-invasive techniques need to be utilized to study organization of lipid and protein assemblies in cell membranes to observe functional 'rafts'. If rafts are to be defined as functional assemblies in cell membranes whose primary 'glue' is lipidic interactions, biophysical methodologies are required to 'observe' these structures. There have been many attempts at developing such techniques, with varying degrees of success. Diffusion methods [29,30] and probe partitioning studies [13] have long been used in living cells to examine lipid and protein heterogeneity in cell membranes. While both studies have provided valuable insights about lipid rafts in cell membranes (reviewed elsewhere in this volume), this review focuses on a different biophysical approach that employs fluorescence imaging of live cells using FRET. The FRET methodology employs fluorescently labeled isoforms of biomolecules to detect extremely short range interactions between the labeled species. It is a non-invasive methodology in so far as fluorescent tags necessary to observe FRET do not perturb the function and distribution of the proteins under observation.

2. Observing molecular interactions beyond optical resolution

Segregated regions at the micron scale of putative lipid raft molecules have not been observed even at the limits of optical resolution set by the intrinsic wave nature of light (Rayleigh criterion), both conventional fluorescence microscopes as well as modern state of the art confocal microscopes (single- and multiphoton excitation) [31]. This implies that rafts must be smaller that the diffraction limit of conventional optical microscopes, 300 nm.

The experimental strategies employed thus far are based on the picture of segregated regions of sphingolipids and cholesterol which contain other lipids and proteins as "solute" particles. Given the difficulty in observing these specific lipid domains on the surface of living cells, it might appear useful to reverse the experimental strategy—first, attempt to determine the nature of the "solutes" and their local organization and then use this to build up the larger lipid "solvent" organization.

In native cell membranes, methods designed to detect proximity between molecules have observed inhomogeneous distributions of many molecular components of rafts, including GPI-anchored proteins. Two types of methods have been deployed for this purpose, biochemical methods utilizing cross-linkers to preserve non-random associations of proteins maintained by labile lipidic interactions, and biophysical methods chiefly FRET. Chemical cross-linking with short (1.1 nm) crosslinkers [32] suggest that cholesterol-sensitive complexes of GPI-anchored proteins exist at the cell surface containing anywhere from 2 to 14 molecules. These experiments were conducted using non-specific cell-impermeant cross-linkers at low temperatures for extended period of time. While this procedure facilitates detection of relatively long-lived pre-existing structures, it is difficult to quantify the actual size or abundance of pre-existing clusters in the membrane. Nevertheless these methods have provided new insights into Golgi sorting of GPI-anchored proteins, As recently shown by Zurzolo and co-workers, GPI-anchored proteins form large scale complexes in the Golgi, necessary for their traffic to the cell surface [33]. These approaches developed predominantly by the use of new methods in chemical cross-linking, are certainly going to provide alternative ways to observe non-random association of proteins. Likewise, photoaffinity cross-linking with suitable probes attached to lipids and other ligands is also becoming popular to define nearest neighbors and their modulation by altering lipid composition.

The other proximity method that lends itself to quantification depends on the principle of Forster's resonance energy transfer (FRET). The use of FRET has greatly enhanced the detection of intermolecular interactions at scales smaller than 10 nm, approaching a single molecule scale (reviewed in [34]). This technique has been widely used to examine protein–protein and lipid–lipid interactions over the years [35–37], and its application to understanding membrane heterogeneities in living cell membranes has met with some degree of success [38,39].

2.1. Forster theory of FRET

FRET is a quantum mechanical property of a fluorophore resulting in non-radiative energy transfer between the excited state of the donor fluorophore and a suitable acceptor fluorophore via dipole–dipole interactions (see Fig. 2A) [40].To this end, we begin with a discussion of Forster's theory of resonance among neighboring fluorophores, the probability of resonance depends on the local configuration of fluorophores and therefore can be used as "spectroscopic ruler" [41].

All consequences of fluorophore interactions and the range and orientation dependence may be traced to this dipole - induced dipole interaction; energy transfer efficiency depends on the relative orientation and separation between the two transition dipoles as well as on the overlap between donor emission and acceptor absorption spectra [Eqs. (1)–(3)].

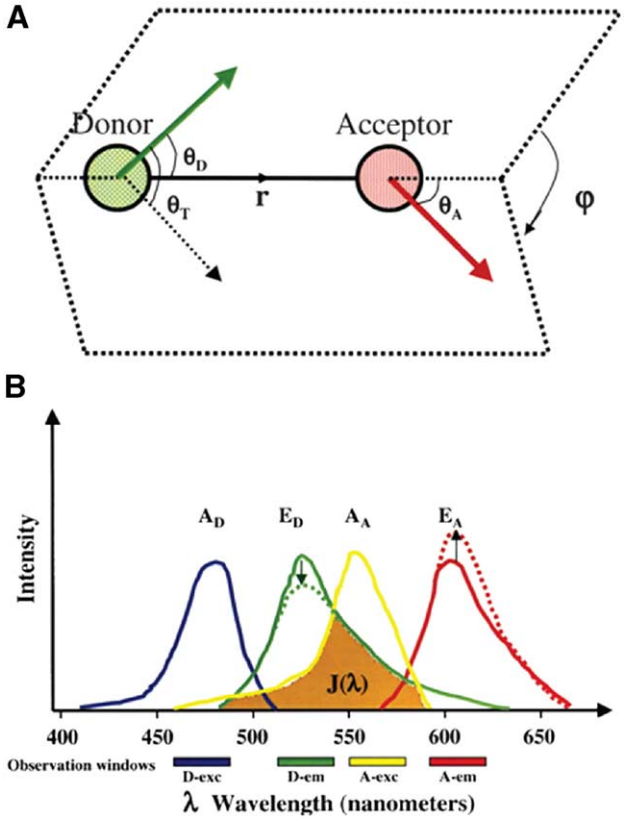

Fig. 2. Schematic depiction of the fluorescence resonance energy transfer process and its implementation. (A) Orientation of donor and acceptor transition dipoles. The relative angle between the two transition dipole is responsible for depolarization of fluorescence upon energy transfer. (B) Overlap integral $J(\lambda)$between the donor emission (E_D) and acceptor absorption spectra (A_A). A_D and E_A are the donor absorption and acceptor emission spectra, respectively. Arrows depict decrease in donor emission and increase in acceptor emission intensities upon energy transfer. Observation windows show excitation and emission wavelength bandwidths for a typical imaging experiment, indicating the potential for cross-talk between the different imaging channels. D, donor; A, acceptor; exc, excitation; em, emission. (reprinted with permission from Ref. [34]).

Simply put, the transfer efficiency varies inversely as the sixth power of the distance between the donor and acceptor [41],

$$E = 1/\left[1 + (r/R_0)^6\right] \quad (1)$$

where r is the distance of separation between the donor and the acceptor fluorophore. R_0 ("Forster Distance") is defined as that separation for which the energy transfer efficiency is 50% and is calculated using the following expression:

$$R_o = \left[8.8.10^{-23}.n^{-4}.Q.\kappa^2.J(\lambda)\right]^{1/6} \quad (2)$$

where, n is the refractive index of medium in the range of overlap, Q is the quantum yield of the donor in the absence of acceptor, $J(\lambda)$ is the spectral overlap as shown in Fig. 2B. κ^2 is the orientation factor which depends on the relative orientation of the two dipoles (Fig. 2A) and is defined by

$$\kappa^2 = [\mathrm{Cos}\ \theta_T - 3\mathrm{Cos}\ \theta_A.Cos\ \theta_D] \quad (3)$$

In general, this orientation factor can vary from 0 to 4 but is usually taken to be 2/3, a value corresponding to a uniformly random orientation of the donors and acceptors. Unless explicitly determined by measurements of fluorescence anisotropy [42], it is often erroneous to assume a value for κ^2, since this may result in significant errors in the measurement of distances [43]. Typically, R_0 varies between 1–10 nm for various pairs of fluorophores [41]; FRET between different spectral variants of GFP fluorophores provide a molecular scale in the range of 2 to 6 nm [44].

Using the expression for the energy transfer efficiency and a statistical distribution of fluorophores, we may arrive at an expression for the probability of non-radiative transfer between any pair in an assembly of fluorophores.

2.2. FRET experimental techniques

Having arrived at an estimate of the likelihood of an excited fluorophore transmitting the excitation to a neighbor, we can use this to formulate experimental strategies to determine the short range organization of fluorophores on the surface of living cells.

The energy transfer event results in different consequences for distinct donor and acceptor fluorophore species that participate in this interaction, namely (i) quenching of donor fluorescence (Fig. 2B); (ii) sensitized emission of the acceptor (Fig. 2B); (iii) reduction in donor lifetime; (iv) increase in donor fluorescence emission anisotropy; (v) depolarization of sensitized acceptor emission.

Obviously the design of a FRET experiment depends on which of the consequences is being monitored [37,45]. In the case of steady state fluorescence emission methods (i, ii, iv, and v) in general for imaging purposes, this translates into collecting an image of donor fluorescence and a separate image of acceptor fluorescence (i and ii) or anisotropy images of donor (iv) or acceptor (v). The ratio images of donor fluorescence to acceptor fluorescence is then compared to the ratio of donor fluorescence to acceptor fluorescence collected under conditions where there is no likelihood of FRET between donor and acceptor. The use of ratio imaging is particularly important since this will take care of local variations of donor and acceptor fluorescence [46,47].

In the simplest situation, the extent of donor quenching may be taken as a good measure of FRET efficiency (E) and this can be calculated from the relative fluorescence yield in the presence (F_{AD}) and in the absence (F_D) of the acceptor.

$$E = 1 - [F_{AD}/F_D] \quad (4)$$

Another experimental determination of donor quenching is by measuring the extent of dequenching upon acceptor photobleaching (reviewed extensively in [37,48]), this is a very useful technique as it directly yields energy transfer efficiencies and is generally unaffected by environmental factors. The extent of increase in donor fluorescence post-bleaching is used to calculate energy transfer efficiencies given by Eq. (4) where now F_{AD} is the fluorescence yield of the donor in the presence of and F_D after photobleaching the acceptor. This method has been used repeatedly to examine the local distribution of raft-associated molecules at the outer leaflet and inner-leaflet [49–51].

A frequently used means of detecting FRET is to directly observe sensitized emission of the acceptor [52,53]. Though straightforward in concept (Fig. 2B) and easy to implement, this experimental paradigm has a lot of practical problems when used for imaging FRET. The choice of the excitation and emission wavelength bandwidths is critical. This is because the sensitized emission signal collected is a composite of (i) fluorescence due to the direct excitation of the acceptor at the donor excitation wavelength, (ii) spill over fluorescence from the donor into the acceptor fluorescence channel, (iii) auto-fluorescence, and finally (iv) a contribution from sensitized emission signal (Fig. 2B). 'Cross-talk' corrections can be difficult to implement and if not done appropriately might mask the energy transfer signal completely [54,55]. A general rule of thumb is that the energy transfer signal should be at least above 10–15% of the total signal observed in the acceptor channel, and be relatively free of cellular autofluorescence.

A consequence of FRET between spectrally distinct donors and acceptors is that donor species are depleted from the excited state by the FRET process, thus the fluorescence lifetime of the donor species is reduced. Energy transfer efficiency (E) may also be directly calculated from the fluorescence lifetime of the donor in the presence (τ_{AD}) or absence (τ_D) of the acceptor as

$$E = 1 - [\tau_{AD}/\tau_D] \quad (5)$$

This may be directly measured via a recently evolving and powerful methodology called Fluorescence Lifetime Imaging Microscopy (FLIM) [36,56,57]. There are two methods of measuring fluorescence lifetimes; a time domain method and a frequency domain method. In the time domain, fluorescence decays are directly measured after exciting with a short pulse of light; the most common technique used is time correlated single photon counting. In the frequency domain, the sample is excited with a light wave whose intensity oscillates sinusoidally with a range of frequencies in the region of the reciprocal of the lifetime that is being measured. The intensity of fluorescence emitted will also vary sinusoidally with the same frequency but with a different phase and amplitude, which may be used to calculate phase τ and modulation τ_M lifetimes. The main advantage of the FLIM technique is that the FRET signal depends only on the excited state reactions and not on the donor concentration or light path length. However, this method requires involved instrumentation [36,56,57].

An indirect consequence of the change in excited state lifetimes is a reduction in the number of donor fluorophores in the excited state. This reduces the rate of photobleaching of the donor species, specifically in the presence of the acceptor species. This has been exploited by Jovin et al. [37], in a method called photobleaching FRET (pbFRET), wherein the photobleaching rate of the donor is measured.

2.3. General homo-FRET microscopy

In conjunction with others, our laboratory has developed a different methodology for performing FRET microscopy in cells, termed homo-FRET [38,58,59]. This method utilizes another well-known consequence of FRET, namely concentration-dependent depolarization of fluorescence [60]. When donor fluorophores are excited with plane polarized light and their rotational diffusion times are longer than the lifetime of the fluorophore, they emit fluorescence which is relatively polarized [61] (Fig. 3A) in the plane containing the axis of the donor dipole and the direction of propagation of the radiation. However, if it transfers energy to neighboring acceptors, even if they are of the same species, the sensitized emission from the 'acceptor' will appear depolarized, due to the large allowed angular spread for this transition (Eq. (3); see also Fig. 2A). The depolarization that the incident polarized light suffers, both due to rotational diffusion and this resonance energy transfer is best measured by the fluorescence anisotropy, A, where

$$A = \frac{I_{||} - I_{\perp}}{I_{||} + 2I_{\perp}} \quad (6)$$

and $I_{||}$ and $I_{\perp}$ are the intensities of emitted light resolved parallel and perpendicular to the incident polarization.

The value of the measured anisotropy depends on the statistical distribution of the relative orientations of the fluorophore dipole moments with respect to the incident polarization and to each other, the rotational diffusion coefficient and the relative separation between fluorophores. The anisotropy is very sensitive to the relative orientation of the dipole moments, thus even if the relative distance between fluorophores is slightly greater then R_0 there is an appreciable depolarization if the dipole moments of the two fluorophores are not parallel to one another. It is a simple exercise to show that $A=0.4$ if the donor dipoles are distributed uniformly over a sphere [61] and there is no energy transfer.

This method is ideally suited for monitoring homo-transfers between like fluorophores, since FRET will cause a net decrease in steady state emission anisotropy (Fig. 3A; [62,63]). However, it may also be used to measure hetero-FRET using similar formalisms.

The efficiency of FRET in this case is simply given by

$$E = 1 - [r/r_0] \quad (7)$$

where r and r_0 are the anisotropy of donor fluorescence in the presence or absence of FRET conditions for the homo-transfer event, respectively. Eq. (7) is valid only under the simplest situations where the sole reason for the change in anisotropy may be attributable to non-radiative transfer to other donor species, where excitation after leaving the donor never returns to the same donor species, and where there is no change in the donor lifetimes [62].

Instrumentation required for anisotropy measurements can be easily implemented in a conventional microscope with the proper placement and alignment of excitation and emission polarizers [38] (Fig. 3D). Since fluorescence anisotropy is an intrinsic property of fluorescence emission, it is independent of the light path and other environmental parameters that affect fluorescence intensity measurements. A requirement of the homo-FRET method is that the donor fluorophore must

have a non-zero value of anisotropy to begin with, and the neighboring 'acceptor' species must have a relatively random orientation and/or some rotational freedom to register sufficient depolarization of fluorescence emission [63]. Fluorescence emission anisotropy is also sensitive to the viscosity of the environment and the mass attached to the fluorescent probe [61], since these factors affect the rotational rates. In practice, the determination of the actual transfer efficiencies by this method may be complicated by several factors [62].

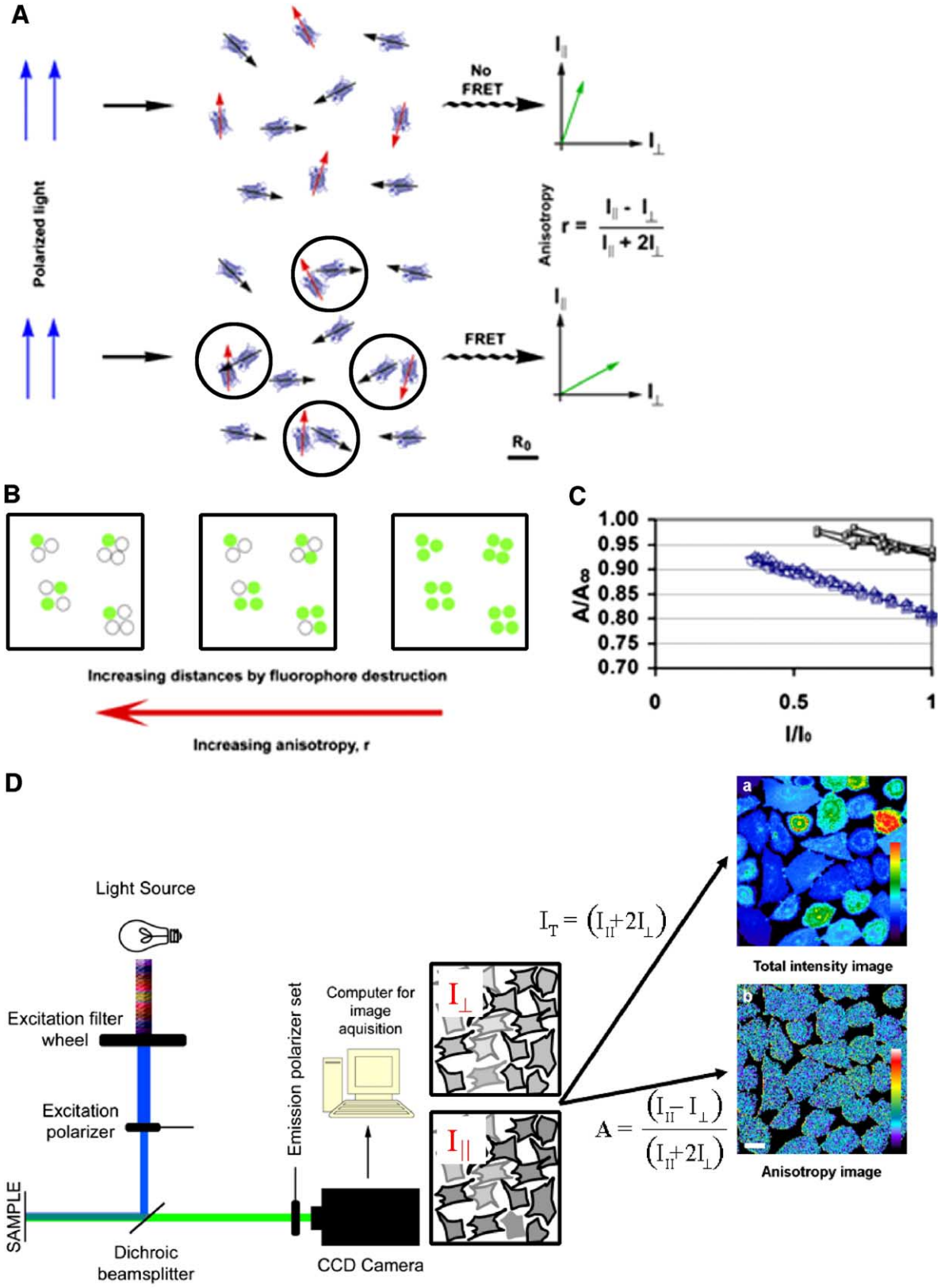

This method is particularly advantageous while probing organizations such as small clusters at membrane surfaces, in the cytoplasm, or in solution [38,58,59,63]. When a single fluorophore is used for labeling, every molecule is capable of being both donor and acceptor thus the probability of FRET between molecules in a small cluster is very high [39,59]. A large variety of fluorophores should be capable of undergoing homo-FRET, thereby allowing the measurement of homo-FRET and with different Forster's radii suitable for uncovering distances in the 2 to 6 nm range [44]. GFP has recently been shown to be a suitable probe for homo-FRET [39,59] providing a useful tool to study the organization of many GFP-tagged proteins inside cells at FRET-scale resolution.

It should also be possible to implement these measurements in a confocal arrangement, allowing visualization of nanometer scale interactions between proteins in intracellular compartments [64]. It should be noted that anisotropy of fluorescence emission is sensitive to the mode of excitation; single and multiphoton excitation may result in different anisotropy scales [65].

3. FRET microscopy and rafts: extending the FRET scale

Our work follows homo and hetero-FRET signatures of lipidic assemblies in live cells [39]. We were able to investigate the size and nature of lipid-dependent organization of GPI-anchored proteins in live cells using these approaches coupled with comparison with theoretical predictions for the perturbation of FRET efficiencies. These perturbations were obtained after photobleaching fluorophore-labeled GPI-anchored proteins folate receptor (FR-GPI) and GFP-tagged to GPI-moiety (GFP-GPI).

To study the organization of GPI-anchored proteins three important parameters had to be established, (i) that GPI-anchored proteins do not give a homo-FRET signal due to high levels in the membrane, (ii) the fraction of proteins engaged in homo-FRET, (iii) the size of (or number of molecules in) the clusters. As detailed in Sharma et al. [39] and in Varma and Mayor [38], GPI-anchored proteins exhibited depolarized emission anisotropy consistent with significant homo-FRET at densities as low as 100/μm^2, to the highest levels obtained in cells by ectopic expression of these construct (2000/μm^2). At these densities, the average protein densities would be too low to exhibit any significant homo-FRET, suggesting that the observation of homo-FRET was consistent with anomalous and heterogeneous distribution of these proteins in the plane of the membrane.

3.1. Modeling FRET experiments

After photobleaching or quenching fluorophore-tagged GPI-anchored proteins, we observed that emission anisotropy increased in a systematic fashion (Fig. 3C). We then interrogated two types of theoretical models to help explain the organization necessary to obtain experimental anisotropy values (Figs. 4 and 5)). These models (in our view) encompass the gamut of possibilities available for arranging proteins in rafts. One class of models considered (Fig. 4A) is consistent with a common picture of rafts where proteins (or a fraction thereof) are arranged in large (tens of nanometer) sized clusters (significantly larger than R_0). The other class of models considered molecular-scale clusters comparable to Forster's radius, potentially accommodating only two to at most four proteins (Fig. 5A).

An additional independent parameter that needed to be ascertained was protein density in the 'raft' to firmly fix the nature of the change in FRET efficiencies upon photobleaching. For this purpose, we extended the homo-FRET experiments to the time domain (Fig. 6). In the time domain, measuring the rate of decay of fluorescence anisotropy directly measures FRET efficiencies. This is related to average distances between GFP-tagged species by the following equation;

$$\omega = \frac{2}{3}\kappa^2\left(\frac{R_0}{R}\right)^6\tau_F^{-1} \tag{8}$$

where the anisotropy decay rate due to homo-FRET, $\tau_{r1}=(1/2\omega)$, τ_F=average fluorescence lifetime and $\kappa^2=2/3$. In case there are multiple anisotropy decay components, the amplitude of the decay component due to FRET also indicates the fraction of molecules undergoing FRET [59]. Thus, by analyzing the rates of anisotropy decay of GFP-tagged GPI-anchored proteins we not only obtain an average distance between GFP-tagged species engaged in homo-FRET, but also the fraction of species engaged in FRET (see Table 1 in Ref. [39]).

Using a more conventional raft-model wherein these proteins are organized in large scale domains (>10 nm, with multiple GPI-anchored proteins present in each domain at experimentally determined local densities of these proteins from time resolved anisotropy decay analyses), we were unable to 'fit' changes in homo-FRET efficiencies obtained after photobleaching the fluorescence (Fig. 4). These results thus rule out most of the expected 'raft' models for GPI-anchored proteins where the size of domains are larger than 10 nm as proposed by many scientists working in this area. A model for a lipidic assembly where a fraction of GPI-anchored proteins were arranged in clusters of the scale of the Forster's radius

Fig. 3. (A) Steady state fluorescence emission anisotropy characteristic of fluorophores that are isolated enough that they do not undergo FRET (top) compared to fluorophores that are in close enough proximity to give rise to FRET, giving rise to a lower value of fluorescence anisotropy (below). (B) Schematic view of the effect of photobleaching on fluorophores (green circles) and fluorescence anisotropy for molecules present in clusters. (C) Experimentally determined change in emission anisotropy, A (with respect to that at infinite dilution, A_∞), of PLF-labeled FR-GPI (triangles) or GFP-GPI (squares) upon fluorophore destruction by photobleaching or chemical quenching, respectively. Intensity at any time (I) was plotted relative to starting value of fluorescence intensity (I_0) for a single cell. Data were obtained for ≥20 cells for each point in the graph. (D) Schematic of imaging setup used to measure steady state anisotropy. Parallel ($I_{||}$) and perpendicular ($I_\perp$) fluorescence intensity images are obtained using a set of excitation and emission polarizer as indicated. Perpendicular and parallel intensity image thus obtained are mathematically processed to obtain anisotropy and total intensity images. Total intensity (a) and anisotropy (b) images of a single field of CHO cells expressing GFP-GPI are shown as pseudo-colored 8-bit images. [panels A–C were adapted from Supplementary text in Ref. [39], with permission].

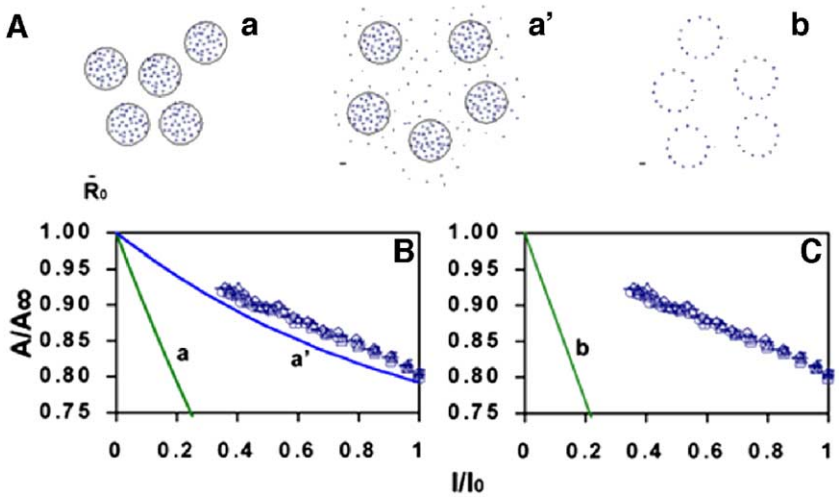

Fig. 4. (A) Models of organization of GPI-anchored proteins. *Model a:* GPI-anchored proteins are uniformly distributed within domains of radii $R>>R_0>l$ (l = molecular size). Model a′: A fraction of the GPI-anchored proteins are organized as in model a, while the remaining are dispersed as isolated fluorophores on the cell surface. Model b: GPI-anchored proteins are distributed uniformly on the periphery of domains of radii $R>>R_0>l$. (B, C) Comparison of relative anisotropy profiles (A/A_∞) versus total intensity, I (relative to its value before photo-bleaching, I_0), calculated from models a (B; green line) and a′ (B; blue line) and b (C; green line) using Forster's theory with experimental anisotropy profiles (symbols) determined from cells expressing different levels of GPI-anchored proteins obtained after photo-bleaching PLF-labeled FR-GPI. The profiles representing models a, a′ and b were calculated with parameters which best fit the entire data set while fixing the average intermolecular distance as 1.2 R_0 between fluorophores within domains for models a and b, and 0.91 R_0 for model a′ with 30% of fluorophores in domains (for a′). Note models a, a′ or b fail to describe the experimental data. [Figure adapted from Ref. [39], with permission].

was able to best describe the experimental data (Fig. 5), providing a picture of how GPI-anchored proteins are arranged in cells at the nanoscale.

3.2. Comparison between homo-FRET and hetero-FRET

The detection of homo-FRET [38,39] but not hetero-FRET [50,51,66] between GPI-anchored proteins requires a consistent explanation. Therefore, we constructed theoretical models based on a probabilistic approach to calculate the extent of hetero-FRET observable from varying fractions of small clusters of molecules that ranged in size from 2 to 7 molecules per cluster. The resultant hetero-FRET efficiencies expected from these models are shown in the curves in Fig. 7. In comparison with experimentally detected FRET efficiencies at these densities of molecules in the membrane, they provided

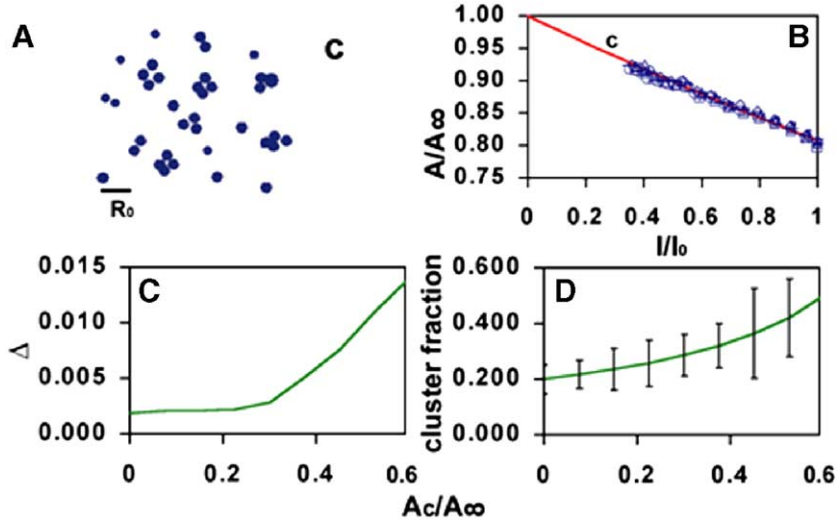

Fig. 5. (A) Model c: GPI-anchored proteins are distributed as a collection of monomers (isolated proteins) and n-mers (with $n>2$), with inter protein distances within an n-mer of the order of R_0, Forster's radius (Scale bar). (B) Comparison of experimental anisotropy profiles (symbols) determined from cells expressing different levels of GPI-anchored proteins obtained after photo-bleaching PLF-labeled FR-GPI with best-fit curve for model c (red line). Fixing the steady state anisotropy of an isolated fluorophore $A^{(1)}=A_\infty=0.247$, and the steady state anisotropy of an n-mer, $A^{(2)}=A^{(3)}=A^{(4)}=0.1$ $A^{(1)}=A_C$, and $A^{(n)}=0$ when $n>5$, we find that 22% of fluorophores are present in clusters. (C) Varying A_C, the steady state anisotropy of a cluster, we determine the best fit and the standard deviation Δ for the fraction of clusters among the anisotropy profiles of individual cells from a single dish. For values of $A_C/A_\infty<0.35$ model c shows a good fit with the data. (D) Cluster fraction (line) at different values of A_C is the best-fit to data collected over cells present in 10 different dishes. Vertical error bars correspond to the standard deviation in the cluster fraction. Given the optimum value of A_C/A_∞ we find that the range in the cluster fraction can be anywhere between 20% and 40%. [Figure adapted from Ref. [39], with permission].

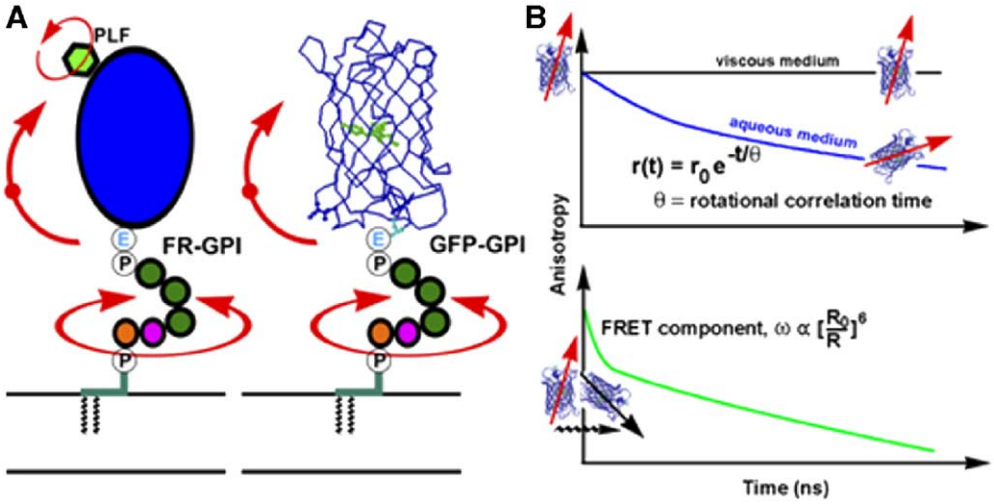

Fig. 6. Panel A shows cartoons depicting the possibilities of rotational motion (red arrows) for the fluorophores, PLF-labeled FR-GPI {human folate receptor (FR-GPI) labeled via a monovalent fluorescent folic acid analog, N-α-pteroyl-N-ϵ-(4′- fluorescein -thiocarbamoyl)-L-lysine (PLF)}, and GPI-anchored Enhanced Green Fluorescent Protein (GFP-GPI or variants of GFP, mCFP- and mYFP-GPI). Panel B shows the expected time-resolved anisotropy decay profiles for dilute GFP-fluorophores (upper panel) immobilized in glycerol solution (viscous medium, black line) or freely rotating in an aqueous solution (blue line). Fluorophores undergoing FRET (green line, lower panel) have an additional fast anisotropy decay rate, ω, related to the average distance between fluorophores as described in the text.

another way of putting a limit on the size and fraction of clusters of GPI-anchored proteins. Consistent with the size and fraction of clusters obtained from homo-FRET methods, theoretical models to predict hetero-FRET efficiencies also showed that at the low fraction of clusters in the membrane and at the scale of the clusters (2 to 4 species maximum per cluster), it would be unlikely to expect significant hetero-FRET above background fluctuations in FRET signals at low levels of protein expression in the membrane.

In previous studies on hetero-FRET between GPI-anchored proteins, Edidin and co-workers had indicated a lower bound on what could be potentially hidden from detection in the hetero-FRET experiments [50]. They indicated that 'limitations of our current measurements prevent us from ruling out the possibility that FRET between 5′ NT (a GPI-anchored protein: sic) arises from a mixture of a large fraction of randomly distributed and a small fraction of clustered (raft-associated) molecules'. Remarkably, the lower bound for a fraction of clustered proteins set by their modeling studies [50,51] and those independently determined by our hetero-FRET studies [39] are similar.

These studies suggest that in conjunction with a combination of homo- and hetero-FRET measurements, perturbation of FRET efficiencies may be sufficient to model organization at the nanometer scale. This was quite unexpected because typically FRET is expected to provide information in the range of 1 to 10 nm. Potentially, these procedures using advanced imaging techniques and theoretical analyses provide a way to bridge the gap in imaging methodologies at this scale. Similar approaches may be necessary to understand different instances of lipid–lipid and lipid–protein interactions in fleshing out an understanding of rafts in cell membranes.

3.3. Analyzing colocalization at the nanoscale

It was also possible to determine whether the clusters contained single or multiple species using homo-FRET imaging (see schematic in Fig. 8A). The results show that multiple GPI-anchored proteins are present in the same nanocluster. This was a consequence of the ability of untagged GPI-anchored proteins to 'dilute' homo-FRET between fluorophore-tagged species (Fig. 8B), although, hetero-FRET was undetectable.

Studying the organization of inner leaflet proteins, using hetero-FRET (acceptor-photobleaching) microscopy Zacharias and colleagues have shown that monomeric fluorescent protein tagged to lipid-anchors at the inner leaflet exhibit hetero-FRET consistent with anomalously clustered distributions in membranes [49]. The size and structure of these lipidic assemblies remain to be ascertained. From the discussion regarding the comparison between hetero- and homo FRET discussed in Fig. 7, these inner-leaflet structures must be either larger, or present at higher fractions in membranes or both.

4. Unexpected picture of GPI-anchored proteins at the cell surface

FRET studies have provided an unexpected picture of cell surface GPI-anchored proteins (Fig. 5), suggesting that they are present as monomers and a smaller fraction (20–40%) as nanoscale (<5 nm) cholesterol-sensitive clusters. These clusters were shown to be composed of at most four molecules and accommodate diverse GPI-anchored protein species. While crosslinking GPI-anchored proteins is expected to activate signaling via GPI-anchored proteins, we found that cross-linking GPI-anchored proteins segregates these proteins from the pre-existing GPI-anchored protein clusters [39]. These results suggest that induced structures may have different characteristics from the native structures present in the membrane.

An additional surprising feature of the homo-FRET experiments was that the value of the anisotropy (measured over the entire cell surface) was found to be independent of the total number of GPI-anchored proteins expressed by the cell. Using

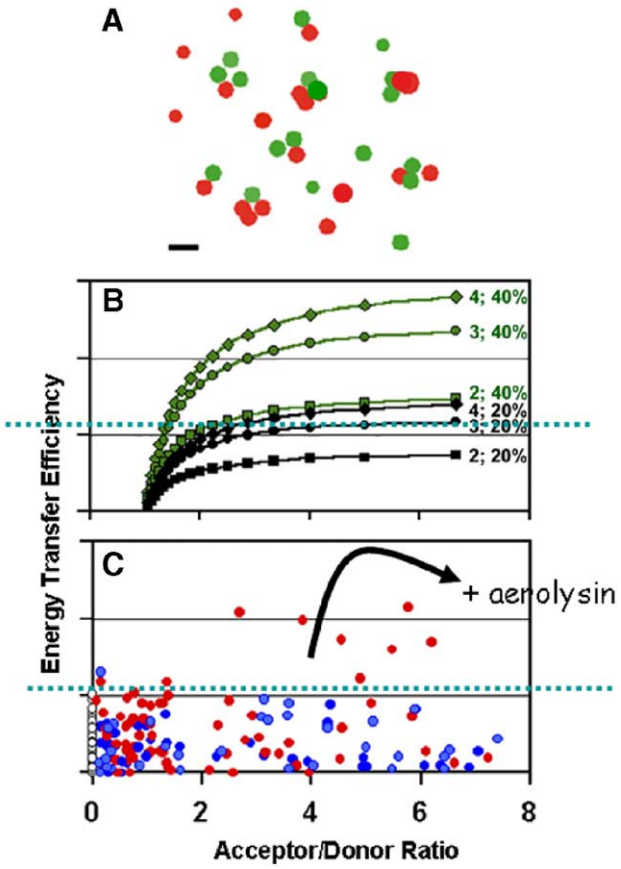

Fig. 7. (A) Schematic showing a possible combination of donor and acceptor fluorophore-species in an arrangement of clusters and monomers at a given donor and acceptor ratio, used for calculations of hetero-FRET efficiencies described below. (B) Efficiencies of energy transfer between donor (mCFP) and acceptor (mYFP) fluorophores species versus different acceptor to donor ratios were explicitly calculated using Forster's theory and combinatorial considerations as applied to model c, wherein the fluorophores appear as monomers and clusters. The values next to each curve in panel B indicate cluster size, n, and percentage of clusters used for determining the energy transfer efficiency. In panel C, energy transfer efficiency was experimentally measured on cells co-expressing different levels of mCFP-GPI and mYFP-GPI. The magnitude of hetero-FRET was determined by analyses of donor dequenching upon acceptor photo-bleaching in the absence (open circles) or presence of acceptor fluorophores (blue circles). Hetero-FRET was also measured on mCFP- and mYFP-GPI-expressing cells incubated with heptamerizing aerolysin toxin [79] to increase the cluster size (red circles). Dotted blue line in panels B and C represent the level of FRET efficiency indistinguishable from control situation where FRET is not expected. [Figure adapted from Ref. [39], with permission].

the proposed model of cluster-monomer organization, this translates to the statement that the relative fraction of clusters to monomers is independent of the total number of GPI-anchored proteins on the cell surface. This can be seen to violate the law of mass action, a necessary requirement of chemical equilibrium and mixing. This surprising observation suggests that the distribution is generated and maintained by specific (nonequilibrium) active cellular processes.

4.1. Implications for lipid–raft structure and function

The observation that GPI-anchored protein clusters exhibit FRET where: i) the capacity of the clusters to undergo exchange (as observed during cross-linking experiments [39]), ii) the observed concentration independence of the steady state anisotropy over a large range of expression levels, implying a fixed proportion of monomers and clusters over this concentration range, brings out an apparent contradiction. Dynamic exchange would result in a distribution of monomers and clusters consistent with chemical equilibrium, but patently inconsistent with the existence of fixed proportion of monomers and clusters. This contradiction may be resolved if nanoscale clusters may be formed in actively generated 'domains' that do not allow for ready mixing. This would suggest that the monomer and cluster distribution is likely to be determined by active cellular processes. The ability of cholesterol levels to modulate the fraction of clusters and monomers suggests that cholesterol homeostasis may in turn regulate this activity.

We have argued that *pre-existing* structures of GPI-anchored proteins at the surface of living cells undergo significant

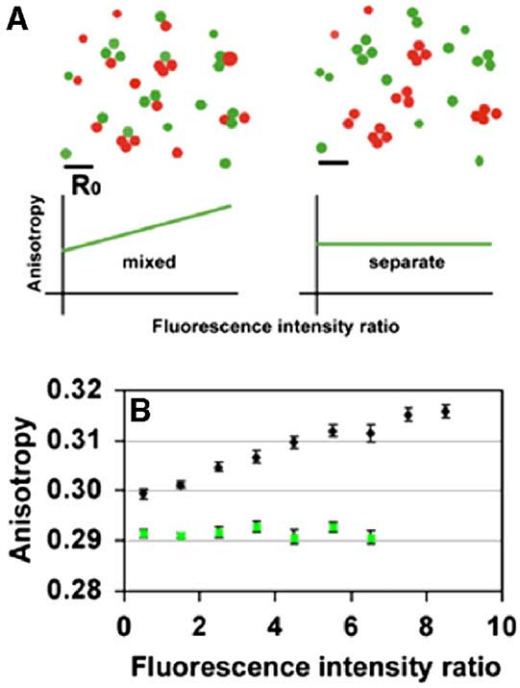

Fig. 8. Multiple GPI-anchored proteins cohabit in the same cluster. A) In the schematic, if two different GPI-anchored proteins (red and green circles) occupy the same cluster (left panel), increasing expression of one GPI-anchored protein (red circles) will lead to decreasing number of homo-FRET events (green circles). As a result, homo-FRET between green species will decrease. Consequently, there will be an increase in emission anisotropy of the fluorescent GPI-anchored protein species being monitored. Alternatively, if different GPI-anchored protein species are present in separate clusters (right panel), there will be no change in the anisotropy of the fluorescent species being monitored with increased expression of one of the proteins. cDNAs encoding GFP-GPI (B) was transiently transfected into FR-isoform (FR-GPI, black circles; FR-TM, green circles)-expressing cells and the fluorescence intensities of Cy5-conjugated Fab fragment of monoclonal antibody Mov19 (Cy5-anti-FR-Fab) and GFP were measured to determine the expression levels of the individual proteins and emission anisotropy of GFP-GPI respectively. Mean values of anisotropy (±S.E.) were determined for ratio ranges (±0.5), and plotted against the midpoint of the corresponding ratio ranges of Cy5-labeled anti-FR-Fab to GFP-GPI. [Figure adapted from Ref. [39], with permission].

reorganization upon cross-linking; the nanoscale clusters are reconfigured and larger and longer-lived cross-linked structures are *induced* with different consequences for endocytosis and signaling [9].

A configuration of molecules consisting of a combination of monomers and small clusters represent a elegant mechanism to combine enhanced binding affinities and a dynamic range of sensitivities [67,68]. Since the cluster/monomers distribution is likely to be determined by an active mechanism in the cell, this suggests that the response behavior of cells will depend on cellular states (e.g., cholesterol homeostasis). This could contribute to the diversification of cellular responses. Nanoscale-clustering also provides a natural explanation for the ability of low concentrations of ligands to efficiently bind GPI-anchored receptors (e.g., heparin sulfate proteoglycans, folate receptors, and cell adhesion molecules), with functional consequences at least in the context of folate transport [69] and integrin function [70]. The presence of multiple GPI-anchored protein species in a tight cluster has potential for tuning the specificity of cell–cell adhesion function since many adhesion molecules are GPI-anchored [71]. As a specific case of 'protein pathology', this nanoscale clustering is likely to be utilized in the conversion of GPI-anchored prion proteins to infectious scrapie [72,73]. The clusters could provide a high density of prion molecules in the plane of the membrane required for efficient conversion to the scrapie form with monomers providing a constant source of substrate for the trans-configuration, providing a potential (structural) candidate for the 'X-factor' involved in scrapie transconfiguration at the cell surface.

5. Conclusion and perspectives

Insights gained from studying the specific case of GPI-anchored protein organization, indicate that this combination of techniques may be used to study other nanoscale organizations that occur frequently in biological processes. For example, understanding the cycle of dynamin-oligomerization during the construction of a coated pit is likely to provide major insight into understanding how dynamin works in the process of vesicle scission. There is considerable controversy over the oligomeric nature of myosin motors, especially myosin VI [74]. To resolve this controversy FRET techniques capable of observing oligomeric states of proteins inside cells are required.

It is increasingly clear that FRET-methodology, such as those described here, will have to be routinely adapted to study lipid-dependent 'raft' organization due to its non-perturbing nature, sensitivity and nanometer resolution. The use of FRET to study the construction of signaling platforms potentially organized by lipidic assemblies is receiving increasing attention. Recent studies on interleukin receptor isoforms [75] and epidermal growth factor receptor oligomerization [76] have provided insights into the dynamic construction of functional assemblies in cell membranes. The FRET approach has also yielded significant advances in understanding organization at T- cell immunological synapse [77]. By the use of FRET sensors, a nanoscale picture of functional lipid assemblies in live cells is emerging [78].

Given the wide range of spatio-temporal scales that the cell surface operates with, it is clear that we will not be able to build a complete picture with just one set of experimental probes (which are best suited for a given scale). Complementary experimental methods coupled with analysis would provide a coherent and complex picture which would fit all scales of observation.

Acknowledgements

S.M. is supported by a Senior Research Fellowship from The Wellcome Trust (grant #056727/Z/99, S. M.), and intramural funding from the National Centre for Biological Sciences. S. M. and M. R. gratefully acknowledge support from Department of Science and Technology (India) via Swarnajayanthi Fellowships. S. M. and M. R. would like to thank their former students, Drs. Sarasij R (NCBS, Bangalore), P. Sharma (CSHL, New York), and R. Varma (Skirball Institute, NYU, New York) for their invaluable contributions to the development of the homo-FRET methodology. S. M. would like to acknowledge G. van der Goot (Univ. Geneva) for her generous gift of aerolysin toxin and Sameera for help with the manuscript.

References

[1] M. Zerial, H. McBride, Rab proteins as membrane organizers, Nat. Rev., Mol. Cell Biol. 2 (2001) 107–117.
[2] J. Rappoport, S. Simon, A. Benmerah, Understanding living clathrin-coated pits, Traffic 5 (2004) 327–337.
[3] V.I. Slepnev, P. De Camilli, Accessory factors in clathrin-dependent synaptic vesicle endocytosis, Nat. Rev., Neurosci. 1 (2000) 161–172.
[4] M.L. Dustin, D.R. Colman, Neural and immunological synaptic relations, Science 298 (2002) 785–789.
[5] K. Simons, G. van Meer, Lipid sorting in epithelial cells, Biochemistry 27 (1988) 6197–6202.
[6] K. Simons, E. Ikonen, Functional rafts in cell membranes, Nature 387 (1997) 569–572.
[7] K. Simons, D. Toomre, Lipid rafts and signal transduction, Nat. Rev., Mol. Cell Biol. 1 (2000) 31–39.
[8] S. Munro, Lipid rafts: elusive or illusive? Cell 115 (2003) 377–388.
[9] S. Mayor, M. Rao, Rafts: scale-dependent, active lipid organization at the cell surface, Traffic 5 (2004) 231–240.
[10] K. Simons, W.L. Vaz, Model systems, lipid rafts, and cell membranes, Annu. Rev. Biophys. Biomol. Struct. 33 (2004) 269–295.
[11] A. Pralle, P. Keller, E. Florin, K. Simons, J.K. Horber, Sphingolipid-cholesterol rafts diffuse as small entities in the plasma membrane of mammalian cells, J. Cell Biol. 148 (2000) 997–1008.
[12] R.G. Anderson, K. Jacobson, A role for lipid shells in targeting proteins to caveolae, rafts, and other lipid domains, Science 296 (2002) 1821–1825.
[13] F.R. Maxfield, Plasma membrane microdomains, Curr. Opin. Cell Biol. 14 (2002) 483–487.
[14] M. Edidin, The state of lipid rafts: from model membranes to cells, Annu. Rev. Biophys. Biomol. Struct. 16 (2003) 16.
[15] D.A. Brown, E. London, Structure and function of sphingolipid- and cholesterol-rich membrane rafts, J. Biol. Chem. 275 (2000) 17221–17224.
[16] H. Heerklotz, Triton promotes domain formation in lipid raft mixtures, Biophys. J. 83 (2002) 2693–2701.
[17] H. Heerklotz, H. Szadkowska, T. Anderson, J. Seelig, The sensitivity of lipid domains to small perturbations demonstrated by the effect of Triton, J. Mol. Biol. 329 (2003) 793–799.
[18] R.F. De Almeida, A. Fedorov, M. Prieto, Sphingomyelin/Phosphatidyl-

choline/Cholesterol phase diagram: boundaries and composition of lipid rafts, Biophys. J. 85 (2003) 2406–2416.
[19] S. Mayor, H. Riezman, Sorting GPI-anchored proteins, Nat. Rev., Mol. Cell Biol. 5 (2004) 110–120.
[20] J. Kwik, S. Boyle, D. Fooksman, L. Margolis, M.P. Sheetz, M. Edidin, Membrane cholesterol, lateral mobility, and the phosphatidylinositol 4,5-bisphosphate-dependent organization of cell actin, Proc. Natl. Acad. Sci. U. S. A. 100 (2003) 13964–13969.
[21] L.J. Foster, C.L. De Hoog, M. Mann, Unbiased quantitative proteomics of lipid rafts reveals high specificity for signaling factors, Proc. Natl. Acad. Sci. U. S. A. 100 (2003) 5813–5818.
[22] S. Schuck, M. Honsho, K. Ekroos, A. Shevchenko, K. Simons, Resistance of cell membranes to different detergents, Proc. Natl. Acad. Sci. U. S. A. 100 (2003) 5795–5800.
[23] C. Zurzolo, G. van Meer, S. Mayor, The order of rafts, EMBO Rep. 4 (2003) 1117–1121.
[24] P. Sharma, S. Sabharanjak, S. Mayor, Endocytosis of lipid rafts: an identity crisis, Semin. Cell Dev. Biol. 13 (2002) 205–214.
[25] C. Dietrich, L.A. Bagatolli, Z.N. Volovyk, N.L. Thompson, M. Levi, K. Jacobson, E. Gratton, Lipid rafts reconstituted in model membranes, Biophys. J. 80 (2001) 1417–1428.
[26] C. Dietrich, Z.N. Volovyk, M. Levi, N.L. Thompson, K. Jacobson, Partitioning of Thy-1, GM1, and cross-linked phospholipid analogs into lipid rafts reconstituted in supported model membrane monolayers, Proc. Natl. Acad. Sci. U. S. A. 98 (2001) 10642–10647.
[27] C. Dietrich, B. Yang, T. Fujiwara, A. Kusumi, K. Jacobson, Relationship of lipid rafts to transient confinement zones detected by single particle tracking, Biophys. J. 82 (2002) 274–284.
[28] M. Hao, S. Mukherjee, F.R. Maxfield, Cholesterol depletion induces large scale domain segregation in living cell membranes, Proc. Natl. Acad. Sci. U. S. A. 98 (2001) 13072–13077.
[29] K. Ritchie, R. Iino, T. Fujiwara, K. Murase, A. Kusumi, The fence and picket structure of the plasma membrane of live cells as revealed by single molecule techniques (Review), Mol. Membr. Biol. 20 (2003) 13–18.
[30] K. Ritchie, A. Kusumi, Single-particle tracking image microscopy, Methods Enzymol. 360 (2003) 618–634.
[31] M. Edidin, Shrinking patches and slippery rafts: scales of domains in the plasma membrane, Trends Cell Biol. 11 (2001) 492–496.
[32] T. Friedrichson, T.V. Kurzchalia, Microdomains of GPI-anchored proteins in living cells revealed by crosslinking, Nature 394 (1998) 802–805.
[33] S. Paladino, D. Sarnataro, R. Pillich, S. Tivodar, L. Nitsch, C. Zurzolo, Protein oligomerization modulates raft partitioning and apical sorting of GPI-anchored proteins, J. Cell Biol. 167 (2004) 699–709.
[34] R.V. Krishnan, R. Varma, S. Mayor, Fluorescence methods to probe nanometer-scale organization of molecules in living cell membranes, J. Fluoresc. 11 (2001) 211–226.
[35] A. Periasamy, R.N. Day, Visualizing protein interactions in living cells using digitized GFP imaging and FRET microscopy, Methods Cell Biol. 58 (1999) 293–314.
[36] P.I. Bastiaens, A. Squire, Fluorescence lifetime imaging microscopy: spatial resolution of biochemical processes in the cell, Trends Cell Biol. 9 (1999) 48–52.
[37] T.M. Jovin, D.J. Arndt-Jovin, in: E. Kohen, J.G. Hirschberg (Eds.), Cell Structure and Function by Microspectrofluorometry, Academic Press, San Diego, 1989, pp. 99–117.
[38] R. Varma, S. Mayor, GPI-anchored proteins are organized in submicron domains at the cell surface, Nature 394 (1998) 798–801.
[39] P. Sharma, R. Varma, R.C. Sarasij, Ira, K. Gousset, G. Krishnamoorthy, M. Rao, S. Mayor, Nanoscale organization of multiple GPI-anchored proteins in living cell membranes, Cell 116 (2004) 577–589.
[40] T. Forster, Intermolecular energy migration and fluorescence. Surface density, Ann. Phys. 2 (1948) 55–75.
[41] L. Stryer, Fluorescence energy transfer as a spectroscopic ruler, Annu. Rev. Biochem. 47 (1978) 819–846.
[42] R.E. Dale, J. Eisinger, W.E. Blumberg, The orientation freedom of molecular probes, Biophys. J. 26 (1979) 161–193.
[43] P. Wu, L. Brand, Orientation factor in steady-state and time-resolved resonance energy transfer measurements, Biochemistry 31 (1992) 7939–7947.
[44] G.H. Patterson, D.W. Piston, B.G. Barisas, Forster distances between green fluorescent protein pairs, Anal. Biochem. 284 (2000) 438–440.
[45] T.M. Jovin, D.J. Arndt-Jovin, Luminescence digital imaging microscopy, Annu. Rev. Biophys. Biophys. Chem. 18 (1989) 271–308.
[46] G.R. Bright, G.W. Fisher, J. Rogowska, D.L. Taylor, in: D.L. Taylor, Y. Wang (Eds.), Fluorescence Microscopy of Living Cells in Culture (Part B), Academic Press Inc., California, 1989, pp. 157–192.
[47] K.W. Dunn, S. Mayor, J.N. Myers, F.R. Maxfield, Applications of ratio fluorescence microscopy in the study of cell physiology, FASEB J. 8 (1994) 573–582.
[48] A.K. Kenworthy, M. Edidin, in: M.H. Gelb (Ed.), Protein Lipidation Protocols, Humana Press, Totowa, NJ, 1999, pp. 37–49.
[49] D.A. Zacharias, J.D. Violin, A.C. Newton, R.Y. Tsien, Partitioning of lipid-modified monomeric GFPs into membrane microdomains of live cells, Science 296 (2002) 913–916.
[50] A.K. Kenworthy, M. Edidin, Distribution of a glycosylphosphatidylinositol-anchored protein at the apical surface of MDCK cells examined at a resolution of and lt;100 A using imaging fluorescence resonance energy transfer, J. Cell Biol. 142 (1998) 69–84.
[51] A.K. Kenworthy, N. Petranova, M. Edidin, High-resolution FRET microscopy of cholera toxin B-subunit and GPI-anchored proteins in cell plasma membranes, Mol. Biol. Cell 11 (2000) 1645–1655.
[52] G.W. Gordon, G. Berry, X.H. Liang, B. Levine, B. Herman, Quantitative fluorescence resonance energy transfer measurements using fluorescence microscopy, Biophys. J. 74 (1998) 2702–2713.
[53] B. Herman, in: D.L. Taylor, Y. Wang (Eds.), Fluorescence Microscopy of Living Cells in Culture (part B), Academic Press Inc., California, 1989, pp. 220–243.
[54] N. Billinton, A.W. Knight, Seeing the wood through the trees: a review of techniques for distinguishing green fluorescent protein from endogenous autofluorescence, Anal. Biochem. 291 (2001) 175–197.
[55] P. Nagy, G. Vamosi, A. Bodnar, S.J. Lockett, J. Szollosi, Intensity-based energy transfer measurements in digital imaging microscopy, Eur Biophys. J. 27 (1998) 377–389.
[56] T. Oida, Y. Sako, A. Kusumi, Fluorescence lifetime imaging microscopy (flimscopy). Methodology development and application to studies of endosome fusion in single cells, Biophys. J. 64 (1993) 676–685.
[57] H. Wallrabe, A. Periasamy, Imaging protein molecules using FRET and FLIM microscopy, Curr. Opin. Biotechnol. 16 (2005) 19–27.
[58] J.V. Rocheleau, M. Edidin, D.W. Piston, Intrasequence GFP in class I MHC molecules, a rigid probe for fluorescence anisotropy measurements of the membrane environment, Biophys. J. 84 (2003) 4078–4086.
[59] I. Gautier, M. Tramier, C. Durieux, J. Coppey, R.B. Pansu, J.C. Nicolas, K. Kemnitz, M. Coppey-Moisan, Homo-FRET microscopy in living cells to measure monomer–dimer transition of GFT-tagged proteins, Biophys. J. 80 (2001) 3000–3008.
[60] G. Weber, Dependence of polarization of the fluorescence on the concentration, Trans. Faraday Soc. 50 (1954) 552–555.
[61] J.R. Lakowicz, Principles of Fluorescence Spectroscopy, 2nd ed., Plenum Press, New York, 1999.
[62] V.M. Agranovich, M.D. Galanin, Electronic Excitation energy transfer in condensed matter, North Holland Publishing Co., Amsterdam, 1982.
[63] L.W. Runnels, S.F. Scarlata, Theory and application of fluorescence homotransfer to melittin oligomerization, Biophys. J. 69 (1995) 1569–1583.
[64] M.A. Rizzo, D.W. Piston, High-contrast imaging of fluorescent protein FRET by fluorescence polarization microscopy, Biophys. J. 88 (2005) L14–L16.
[65] A. Volkmer, V. Subramaniam, D.J. Birch, T.M. Jovin, One- and two-photon excited fluorescence lifetimes and anisotropy decays of green fluorescent proteins, Biophys. J. 78 (2000) 1589–1598.
[66] O.O. Glebov, B.J. Nichols, Lipid raft proteins have a random distribution during localized activation of the T-cell receptor, Nat. Cell Biol. 6 (2004) 238–243.
[67] D.J. Irvine, K.A. Hue, A.M. Mayes, L.G. Griffith, Simulations of cell-surface integrin binding to nanoscale-clustered adhesion ligands, Biophys. J. 82 (2002) 120–132.

[68] D. Bray, M.D. Levin, C.J. Morton-Firth, Receptor clustering as a cellular mechanism to control sensitivity, Nature 393 (1998) 85–88.
[69] H. Matsue, K.G. Rothberg, A. Takashima, B.A. Kamen, R.G. Anderson, S.W. Lacey, Folate receptor allows cells to grow in low concentrations of 5-methyltetrahydrofolate, Proc. Natl. Acad. Sci. U. S. A. 89 (1992) 6006–6009.
[70] C.V. Carman, T.A. Springer, Integrin avidity regulation: are changes in affinity and conformation underemphasized? Curr. Opin. Cell Biol. 15 (2003) 547–556.
[71] T.J. Harris, C.H. Siu, Reciprocal raft–receptor interactions and the assembly of adhesion complexes, Bioessays 24 (2002) 996–1003.
[72] A. Taraboulos, M. Scott, A. Semenov, D. Avrahami, L. Laszlo, S.B. Prusiner, D. Avraham, Cholesterol depletion and modification of COOH-terminal targeting sequence of the prion protein inhibit formation of the scrapie isoform, J. Cell Biol. 129 (1995) 121–132.
[73] K. Kaneko, M. Vey, M. Scott, S. Pilkuhn, F.E. Cohen, S.B. Prusiner, COOH-terminal sequence of the cellular prion protein directs subcellular trafficking and controls conversion into the scrapie isoform, Proc. Natl. Acad. Sci. U. S. A. 94 (1997) 2333–2338.
[74] R. Roberts, I. Lister, S. Schmitz, M. Walker, C. Veigel, J. Trinick, F. Buss, J. Kendrick-Jones, Myosin VI: cellular functions and motor properties, Philos. Trans. R. Soc. Lond., B Biol. Sci. 359 (2004) 1931–1944.
[75] G. Vamosi, A. Bodnar, G. Vereb, A. Jenei, C.K. Goldman, J. Langowski, K. Toth, L. Matyus, J. Szollosi, T.A. Waldmann, S. Damjanovich, IL-2 and IL-15 receptor alpha-subunits are coexpressed in a supramolecular receptor cluster in lipid rafts of T cells, Proc. Natl. Acad. Sci. U. S. A. 101 (2004) 11082–11087.
[76] P. Nagy, G. Vereb, Z. Sebestyen, G. Horvath, S.J. Lockett, S. Damjanovich, J.W. Park, T.M. Jovin, J. Szollosi, Lipid rafts and the local density of ErbB proteins influence the biological role of homo- and heteroassociations of ErbB2, J. Cell Sci. 115 (2002) 4251–4262.
[77] T. Zal, N.R. Gascoigne, Using live FRET imaging to reveal early protein–protein interactions during T cell activation, Curr. Opin. Immunol. 16 (2004) 418–427.
[78] A. Miyawaki, Visualization of the spatial and temporal dynamics of intracellular signaling, Dev. Cell 4 (2003) 295–305.
[79] Y. Tsitrin, C.J. Morton, C. el-Bez, P. Paumard, M.C. Velluz, M. Adrian, J. Dubochet, M.W. Parker, S. Lanzavecchia, F.G. van der Goot, Conversion of a transmembrane to a water-soluble protein complex by a single point mutation, Nat. Struct. Biol. 9 (2002) 729–733.